




Assessing the Impact of the October 2020 Capena Earthquake on the Lago Puzzo Sinkhole (San Martino Valley, Rome, Italy): Seismological, InSAR, and Geophysical Evidence of Possible Causal Relationships

R. DE RITIS,¹  G. ROTELLA,² C. TOLOMEI,¹ G. CALDERONI,¹ F. MARRA,¹ A. ARGENTIERI,² P. VITALI,² M. FABIANI,² M. CHIAPPINI,¹ and C. DOGLIONI^{1,3}

Abstract—In October 2020, a low-magnitude earthquake struck near the village of Capena, approximately 30 kilometers north of Rome. This seismic event was particularly remarkable due to its shallow hypocenter and the complete absence of aftershocks. Additionally, both during and after the event, residents reported hearing loud rumbling noises on multiple occasions in the village and surrounding rural areas. The earthquake's epicenter is located in a sinkhole-prone region intersected by major infrastructure, including a high-speed railway, high-voltage power lines, and a provincial road. Given these conditions, public authorities and regional Civil Protection agency closely monitored the area, prompting a comprehensive investigation. The study adopted an interdisciplinary approach to assess the stability of sinkhole-prone zones and identify any geological changes potentially triggered by the earthquake. A key focus of the research was the “Lago Puzzo,” a well-documented example of multiphase, still active, sinkhole evolution within the San Martino Valley, alongside other similar extinct features in the area. The investigation integrated three primary methodologies: spectral analysis of seismic data to characterize the October 2020 event; remote sensing (SAR) using InSAR analysis to map ground displacement; geophysical surveys (ERT) to reveal subsurface structures. Although the study found no direct correlation between the earthquake and the evolution of Lago Puzzo, the results provide valuable insights into the current deformation state of the sinkhole and offer projections for its potential future development. Ultimately, this research represents a significant step forward in refining hazard assessment methods for the region.

Keywords: Sinkholes, InSAR and seismological analysis, slope map, electrical resistivity tomography, gravimetry.

1. Introduction

This study was triggered by a low-intensity earthquake that occurred on October 4, 2020 a few hundred meters to the west of the Capena village (epicentral coordinate 42.14°, 12.52°), and by repeated audible noise phenomena perceived by the population for several months during and after the event. These occurrences drew the attention of public institutions. The study area is positioned in the northern sector of the Rome Metropolitan City, between the municipalities of Capena and Fiano Romano (Fig. 1a) and falls within Sheet 365 of the Regional Technical Map (1:10.000 scale), specifically in section 365030 of the 1:5000 scale public Regional Technical Map (CTR, <https://geoportale.regione.lazio.it>).

This is an already known sinkhole-prone area affecting the San Martino Valley (Fig. 1a, b) where depressions, hollows, and lakes occur. The genetic model related to sinkhole formation is sufficiently clear and widely described in the literature (Nisio et al., 2004, Nisio et al., 2007). Generally, these occurrences develop in plains, near tectonic displacement zones, above loose alluvial cover. In these areas, the infiltration of pressurized rising waters from below generates collapsed chimneys composed of voids and liquefied soils. These voids slowly rise to the surface until a sinkhole forms, which is quickly filled by pressurized water, often characterized by an endogenous gas phases (e.g., CO₂, H₂S, CH₄), as confirmed by the sulfur smell reported by many residents.

¹ Istituto Nazionale di Geofisica e Vulcanologia, Rome, Italy.
E-mail: riccardo.deritis@ingv.it

² Dipartimento XI “Geologico - Difesa del suolo e Aree protette” Hub 2 “Sostenibilità territoriale” Città metropolitana di Roma Capitale, Rome, Italy.

³ Dipartimento di Scienze della Terra, Sapienza University, Rome, Italy.

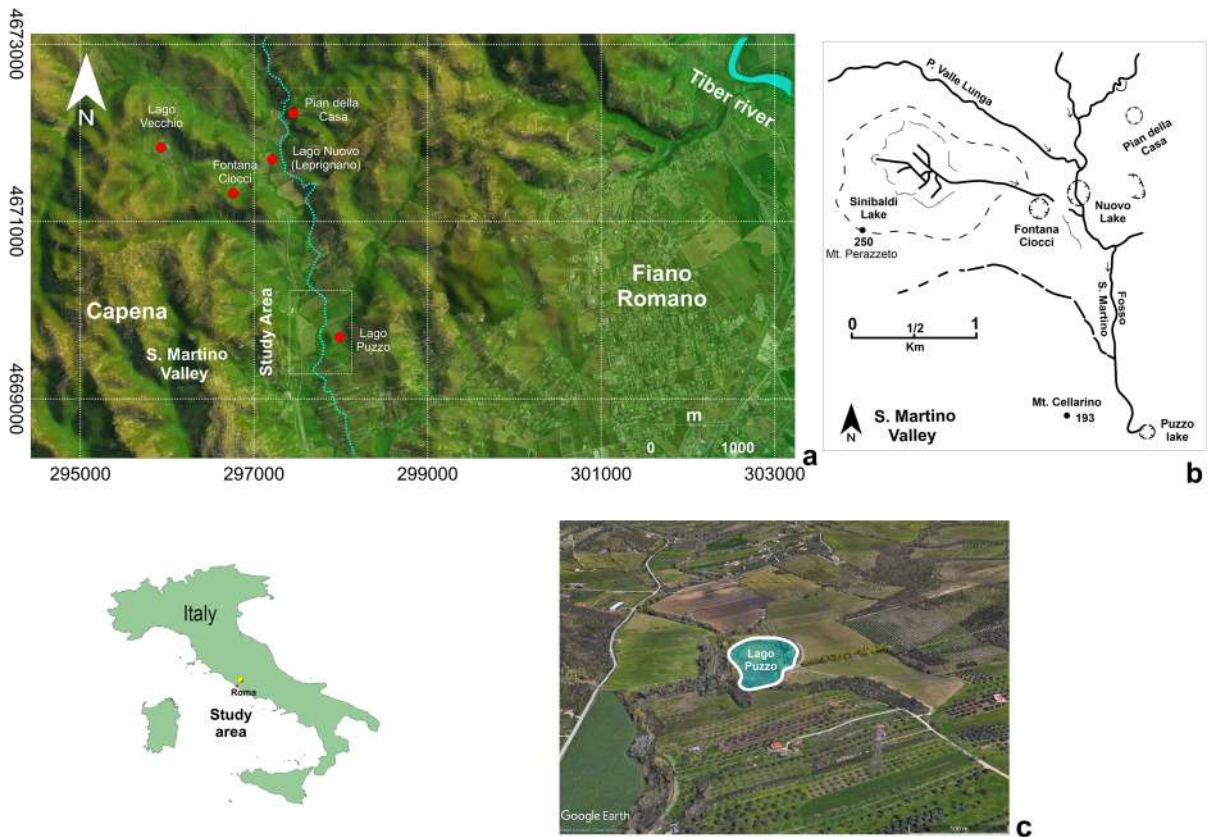


Figure 1

Regional overview of the study area with respect the Tiber valley (a). Fosso di San Martino schema with the main sinkholes mentioned in the text (modifies by Di Loreto et al., 1995, b). Aerial image of the Fosso plateau and the Lago Puzzo plateau viewed from a southern vantage point (Google Earth, c). Study area ubication in the inset

During this study, multiple inspections were conducted across the whole San Martino sinkhole-prone area to identify any surface rupture or ground collapse. Ultimately, attention was focused on the Lago Puzzo active sinkhole to detect possible signs of reactivation, both at the surface and below ground or new formation phenomena Fig. 1c. Furthermore, it is worth mentioning the particular vulnerability of this site because of the occurrence of: (1) a giant power line pylon lying in correspondence of the northern shore of the Lago Puzzo; (2) the high speed Railway crossing about five hundred meters to the west of the lake; (3) several agricultural farms all around the lake; 4) a provincial road (Fig. 8a)

An analysis and interpretation of the collected data and available information was conducted to understand the ongoing geomorphological and

geological dynamics. Particularly, regional gravimetric data were acquired in digital format to model and interpret the local bedrock characteristics (Kaufman, 2014). Moreover, the historical seismicity of the area and the seismic signal recorded by the INGV National network stations during the earthquake of October 4, 2020, were analyzed. An InSAR interferometric analysis of the pre-, co-, and post-seismic phases was also conducted using a pair of SAR images. Subsequently, a geophysical campaign was conducted using Electrical Resistivity Tomography (ERT) in the areas surrounding the Lago Puzzo in order to identify the Lago Puzzo subsurface structure (Walthman et al., 2005, Kaufman, 2014, Argentieri et al., 2015, De Ritis et al., 2020).

This study aimed to identify both surface and subsurface deformation patterns potentially induced

by the earthquake, including associated phenomena and their evolution, with particular emphasis on the lake area. In fact, seismic activity, can play a crucial role in triggering or reactivating sinkholes—especially in karst terrains—through mechanisms such as ground shaking and stress redistribution (Santo et al., 2011; Sella et al., 2014). Understanding these processes is essential for assessing the seismic vulnerability of such geological settings and for improving risk mitigation strategies.

2. Geo-Structural Framework

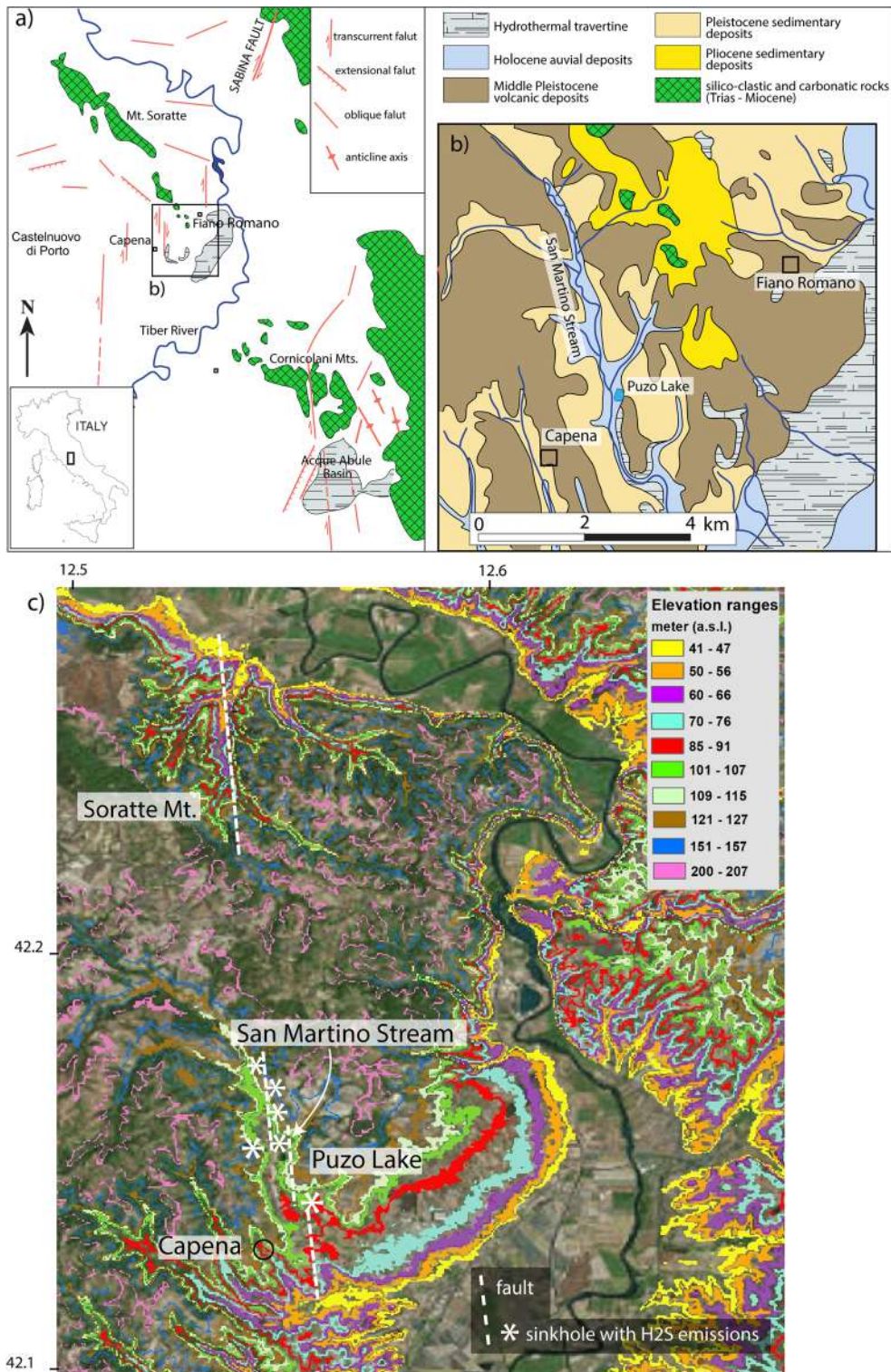
Sinkhole-prone areas share a common predisposing characteristic, specifically, the presence of a bedrock of soluble rocks (e.g., limestone) overlain by alluvial deposits (e.g., cover) generally with poor geo-mechanical properties (Billi et al., 2016 and Reference therein). Along the Tyrrhenian margin of the Apennine chain (central Italy), the carbonate bedrock is downthrown by extensional tectonics beneath terrigenous deposits cover, the volcanic products of the Colli Albani, Sabatini, and Cimini districts (in the upper part of the stratigraphic sequence, Fig. 2a and b, Caramanna et al., 2008). The bedrock regionally hosts large hydrogeological basins with deep circulation, often influenced by mineral species and heat from the cooling of deep magmatic systems related to the aforementioned volcanism. This condition often leads to extensive deep karst phenomena that develop primarily along local and regional faults and fractures, which serve as the main pathways connecting surface water with groundwater (Bense et al., 2013). The buried tectonic framework of the Tyrrhenian margin is characterized by structural highs and lows, both at regional and local scales, forming horsts and grabens. As a result, noteworthy vertical and lateral density heterogeneities are expected within the upper crustal layers. Consequently, the characterization and modeling of geophysical properties can offer valuable insights into the bedrock, including its depth and orientation, the presence of cavities and voids, and the relationship of these latter features with tectonic processes.

The Lago Puzzo is located in the S. Martino Valley, at the eastern edge of the Sabatini volcanic

district and south of the Monte Soratte, on the right bank of the Tiber Valley, which is the local hydrologic base level. The geological context is characterized by deposits of the Plio-Pleistocene marine cycle and volcanic deposits of the Sabatini district. Below these, at depth, lies the Meso-Cenozoic carbonate substrate composed of the calcareous-siliceous units of the Umbrian-Marche stratigraphic sequence (Fig. 2b).

The Monte Soratte is a 4.5 km long, NNW-SSE striking structural horst, bounded by normal faults and interpreted as the result of negative tectonic inversion processes affecting pre-existing surfaces (Faccenna & Funicello, 1993). In particular, tectonic structures observed along its southwestern side (Fig. 2a), consist of marginal faults with limited extension, which do not identify a single tectonic element, but are the surface expression of a crustal N20° striking shear zone (Faccenna & Funicello, 1993). The analysis of the outcropping terrains occurring along the NW-SE trending section of the Fosso San Martino Valley shows the fluvial incision corresponding to a ~N-S striking transtensional fault (Faccenna & Funicello, 1993, Faccenna, 1994). This latter structure, active from the Lower Pliocene to the Lower Pleistocene, is responsible for the presence of a tectonic step already existing during the Pliocene marine transgression (Faccenna & Funicello, 1993).

In the area placed between Castelnuovo di Porto and Fiano Romano (Fig. 2a and b), N-S trending tectonic dislocations affect both the Plio-Pleistocene marine deposits and the volcanoclastic terrains. Kinematic indicators show that these tectonic trends, active during the Middle-Upper Pleistocene, initially exhibited right-lateral strike-slip movement followed by extensional movement under the present-day stress-field (Faccenna & Funicello, 1993). These structures play a role in controlling the surface water circulation, as seen in the N-S trending section of the Fosso San Martino. In this segment, the valley coincides with a shear zone composed of two right-lateral strike-slip tectonic dislocations. Additionally, geomorphological investigations have revealed that NW-SE-oriented river channels are truncated by meridian-flowing watercourses (river captures, Cicacci et al., 1988). The N-S tectonic dislocations are thus superimposed on the NW-SE oriented ones.



Specifically, the direction of the Fosso San Martino, from upstream to downstream, abruptly shifts from

NW-SE, near the southwestern margin of Monte Soratte, to a clearly meridian direction in the study

◀Figure 2

Regional tectonic (modified from Faccenna et al., 1994, **a**) and geological contexts of the investigated area (**b**); DTM image highlighting discrete classes of elevations (modified from Marra et al., 2019) (**c**). See text for comments and explanation. Background image is a freeware by NASA shuttle mission, available under Creative Commons Attribution License (<http://www2.jpl.nasa.gov/srtm>): USGS (2004), Shuttle Radar Topography Mission, 1 Arc Second scene SRTM_u03_n008e004, Unfilled Unfinished 2.0, Global Land Cover Facility, University of Maryland, College Park, Maryland, February 2000

area. In the study area, the structural trends align with the regional N-S and NW-SE orientations, continuing those of M. Soratte, located about 10 km to the northeast.

2.1. Geomorphology

At the regional scale, on the right bank of the Tiber Valley, the MIS 5 terraces (125 ka) are positioned at significantly higher elevations compared to those on the left bank (Marra et al., 2019). This differential uplift has been interpreted as volcanic origin and is associated with the most recent activity of the Sabatini complex (70–100 ka, Peccerillo, 2017). The overlay of the elevation bands (DTM in Fig. 2c) onto the aerial imagery highlights the deformation of the uplifted area (Marra et al., 2019). Along the eastern boundary of this uplifted sector thick travertine layers occur (Fig. 2b, c), likely associated with NNE-SSW trending faults. Additional hydrothermal travertine deposits are also found, during the geological fieldwork carried out as part of this study, between Capena and the study area as well as in the Lago Puzzo.

At the local scale, the Lago Puzzo area is placed along the Fosso di S. Martino, very close the river stream where it receives a north north-eastern tributary. The landscape is characterized by a broad plateau bordered by gently rolling hills with elevations not exceeding 200 meters a.s.l. In this area, the cyclic formation of sinkholes shows a gradual NS migration over time (Pian della Casa, Lago Nuovo, Vecchio, and Fontana Ciocci, located respectively 3.5 km, 2.8 km, and 2 km from Lago Puzzo in Fig. 1a, Nisio, 2008). Some of these structures are no longer

identifiable at the surface but formed and evolved with the same sequence and dynamics. The most recent event is the Lago Puzzo, whose first observed formation dates back to October 28, 1856 (Nisio and Del Prete, 2008), and it is considered an active system.

The morphology, stratigraphy, subsidence, and sinkhole time sequences identify a convergence of predisposing factors within the study area. Particularly, a thick sedimentary cover overlies a shallow carbonate basement, which is influenced by a regional tectonic structure and hydrogeological activity. Aerial pictures analysis and on-field observations revealed the existence of an evident fracture in the ground in the north-eastern side of the lake as well as degassing phenomena on its eastern, south-western and western sides (Fig. 3 c–e). Moreover, the hydraulic head between the Tiber Valley base level and the uplifted Fosso di San Martino sector generates a seasonal driving force for the surficial and groundwater dynamics. This factor convergence increases the probability of future occurrences.

3. Data and Method

3.1. Digital Elevation Model and Aerial Pictures

The morphological analysis was carried out using the publicly available Digital Terrain Model for the area (DTM), specifically the Shuttle Radar Topography Mission dataset (SRTM, <https://www.usgs.gov>), which was made globally accessible by the Jet Propulsion Laboratory (Rodriguez et al., 2005). The SRTM dataset provides high-resolution topographic data for global applications and it has a resolution of 1 arc-second, equivalent to 30 meters.

A sector centered on Lago Puzzo was extracted from the DEM, extending approximately 3 km in the east–west (E–W) direction and 1.8 km in the north–south (N–S) direction (Fig. 3a). Subsequently, the Slope Map was generated (“Slope”, in Fig. 3b). The slope (θ) is defined as the angle of inclination of the terrain at a given point relative to the horizontal plane. It is derived from the DEM using its gradient along the two Cartesian axes. This map represents the spatial variations of the slope angle across the area

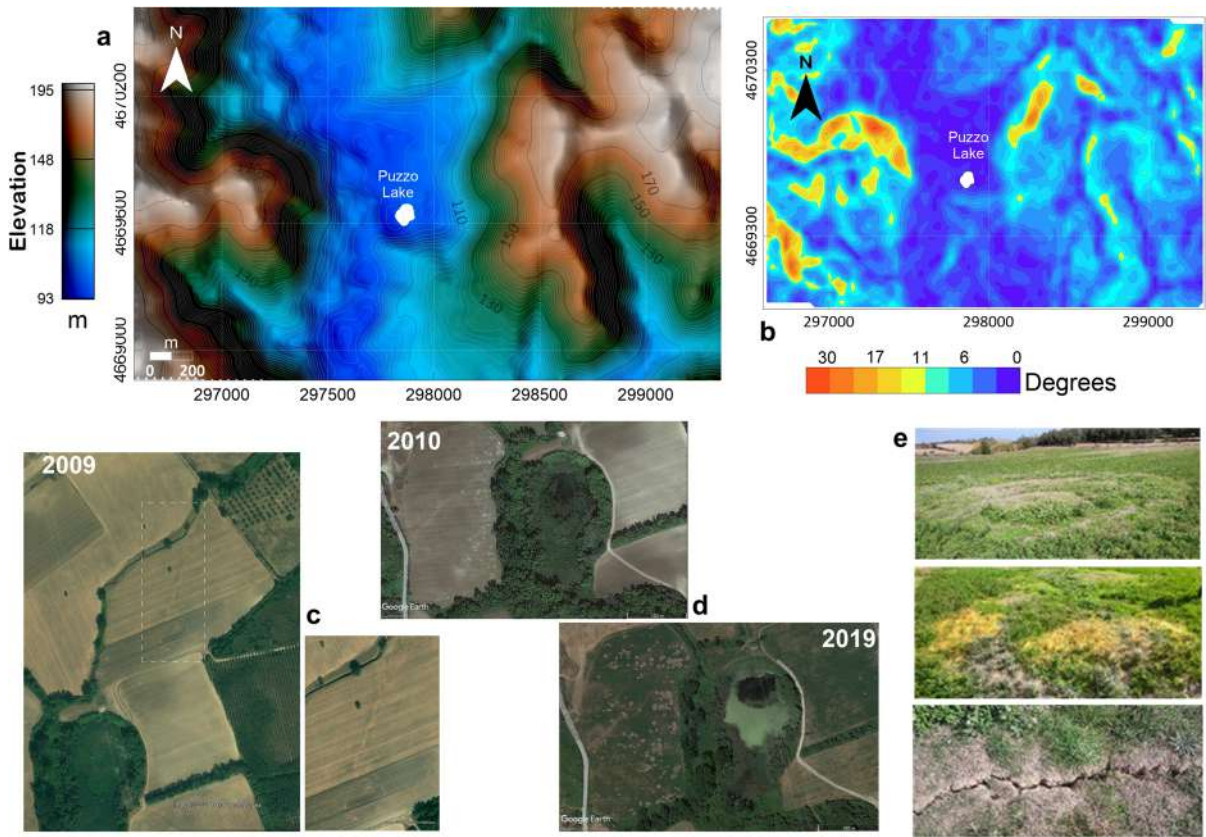


Figure 3

Digital Terrain Model (DTM) of the Lago Puzzo plateau and surrounding hills (a), the Slope map (gradient) of the same area as panel a in color scale indicating the slope as the ratio between the vertical elevation change and the horizontal distance, in degrees (b). Google Earth aerial pictures of the eastern and northeastern sides of the Lago Puzzo plateau showing the NNE-SSW fracturing, zoom in of this latter in the inset, (c), Google Earth pictures with surface footprints of the gas leakage around the Lago Puzzo (d). Photographs of the degassing area on the eastern side of the Lago Puzzo plateau showing the burnt grass as well as the associated fracturing (e)

(ground inclination) measured either in degrees or as a percentage of slope (Micalleff et al., 2011). In this work we measure the Slope in degrees (Fig. 3b).

$$S(\%) = 100 \times \sqrt{\left(\frac{dx}{dy}\right)^2 + \left(\frac{dz}{dy}\right)^2}$$

3.2. Seismic Surveys

3.2.1 Past and Historical Seismicity

The seismicity in the Capena area is sparse and low in magnitude. Instrumental seismicity, recorded by the INGV National Seismic Network from 01/01/1985 to 10/16/2020 within a distance of 10 km from the

Capena earthquake epicenter (Fig. 4) consists of 39 events with local magnitudes (ML) ranging between 0.3 and 3.4 (<http://terremoti.ingv.it/>). The nearest earthquake occurred on 12/04/2010 (ML 1.9), while the strongest was on 07/10/2011, north-east of Sacrofano (ML 3.4). The Parametric Catalogue of Italian Earthquakes (CPTI15, <https://emidius.mi.ingv.it/CPTI15-DBMI15/>) shows the study area does not have a significant seismic history. However, the Tiber Valley has experienced two noteworthy and moderately damaging events: the first occurred on January 19, 1484, though details are sparse; the second was on April 24, 1901. The 1484 earthquake occurred very close to the Capena area and caused unidentified damage (Mentana, Castelnuovo di Porto, Morlupo,

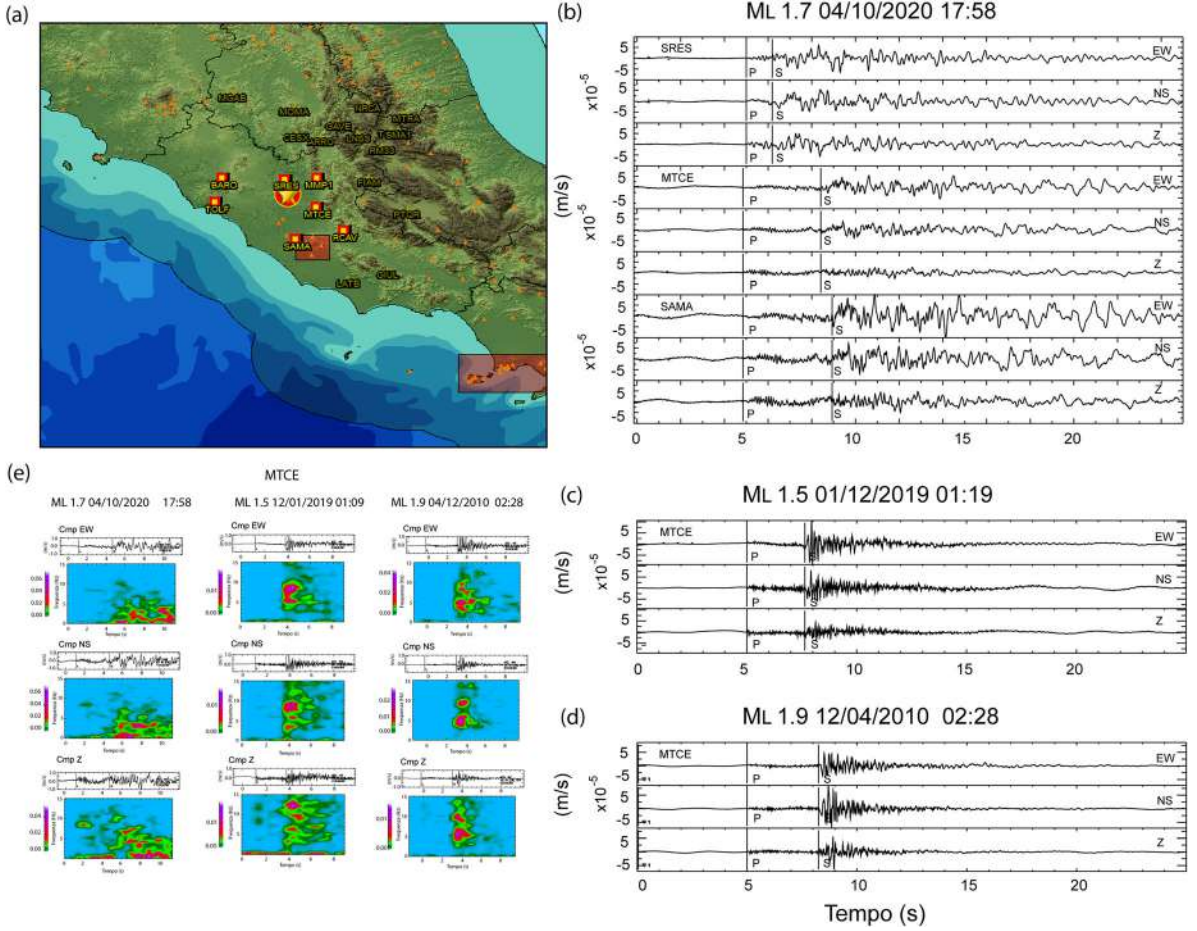


Figure 4

The ML1.7 seismic event (04/10/2020, 17:58 UTC) occurred in Capena (yellow star), with the seismic stations used for its localization highlighted (a). Seismograms of the Capena earthquake recorded at SRES, MTCE, and SAMA. For each station, the three seismic signal components (EW, NS, Z) are displayed. Vertical lines labeled "P" and "S" indicate the arrival times of P and S waves, respectively (b). Seismograms recorded at MTCE for two additional earthquakes in the same area: an ML 1.5 earthquake on 12/01/2020 and an ML 1.9 earthquake on 04/12/2020 (c) and (d). Seismogram and spectrogram recorded at MTCE for: (left) the ML 1.7 Capena earthquake, (middle) the ML 1.9 earthquake, and (right) the ML 1.5 earthquake (e)

and Monterotondo). Instead, the 1901 earthquake, took place at the Monti Lucretili foothills, in an area with thermal activity (Cretone Springs).

3.2.2 October 20, 2020 Earthquake

The INGV Italian Seismic Network located the seismic event of October 4, 2020, at a depth of 5 km, with a hypocenter at Lat 42.14°, Long 12.52° (Fig. 4a). No aftershocks were recorded. The small magnitude (ML 1.7), too low for Time Domain Moment Tensor calculation, did not allow to

determine the focal mechanism of the event. Additionally, the azimuthal coverage of the area's stations also did not grant for focal mechanism determination using first-arrival polarities. Nonetheless, seismic signal analysis of this event revealed several distinctive characteristics (Fig. 4) discussed in the 4.2 paragraph.

3.3. Interferometric Analysis

The SAR data consists of displacement time series and average ground velocity from both ascending and

descending Sentinel-1 satellite orbits (ESA missions). The subsequent InSAR analysis technique utilized the radar satellite images to measure ground displacements with high accuracy (Ferretti et al., 2002, Berardino et al., 2002, Hopper et al., 2004, Nof et al., 2019, Fig. 4). This method can detect vertical movements with sub-centimeter precision and is widely used in seismology. In the study area, the analysis was employed to detect possible deformation fields linked to the described seismic event or any induced phenomena, examining ground movement during pre-, co-, and post-seismic phases. Unfortunately, there are very few Persistent Scatterers (PS) in the proximity of the Lago Puzzo; actually, the closest infrastructures able to reflect the signal are placed several hundred meters from the lake. However, in this latter the ground's average velocity map, and the total deformation have limited variations in magnitude (Fig. 5f, g).

The co-seismic phase analysis was conducted using a pair of SAR images acquired on September 29 and October 5, 2020, respectively. The analysis covered an area of about $100 \times 100 \text{ km}^2$ (Fig. 5a–d). The data were averaged from their original resolution to reduce the typical noise of SAR images, producing two maps where each pixel represents a ground cell of about 30 m. Then, the pre-event analysis was performed by processing SAR images acquired from 2016 to 2020 using the SBAS (Small Baseline Subset, Berardino, et al., 2002) multi-temporal InSAR processing approach. This technique permits us to obtain a time series of ground displacements and the mean velocity m for each coherent pixel over the temporal period covered by the used SAR images. Such an InSAR data analysis allows the detection of ground deformations (along the sensor's line of sight) that occurred at each acquisition with millimeter accuracy. Finally, the post-event analysis was carried out by processing S1 SAR images acquired from 2021 to 2022 using the SBAS processing chain.

3.4. Gravimetry

The regional gravity data was published by the Italian Institute for Environmental Protection and Research (ISPRA - <https://www.isprambiente.gov.it>) and is derived from the integration of onshore and

offshore data for the Italian peninsula, sourced from various organizations such as ENI, OGS, USDMA (U.S. Defense Mapping Agency), and ISPRA itself. The 1:250,000 gravity map of Italy provides Bouguer anomalies for the entire national territory and surrounding marine areas. This map was produced from Free-Air anomalies referenced to the IGSN71 geoid and applying topographic correction (complete Bouguer). The regional field surrounding the study area is shown in Fig. 6a.

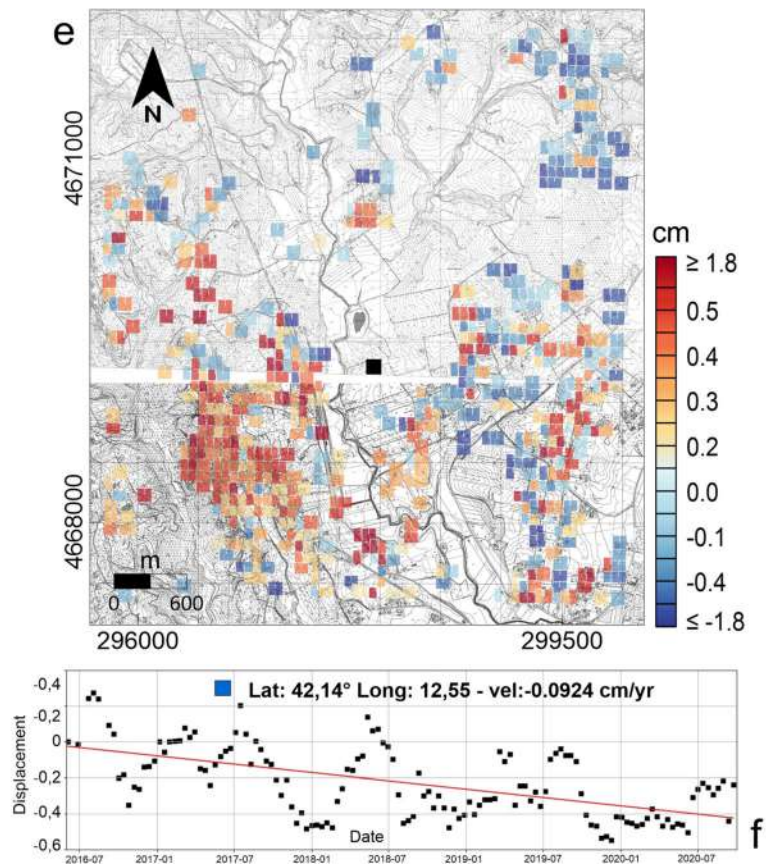
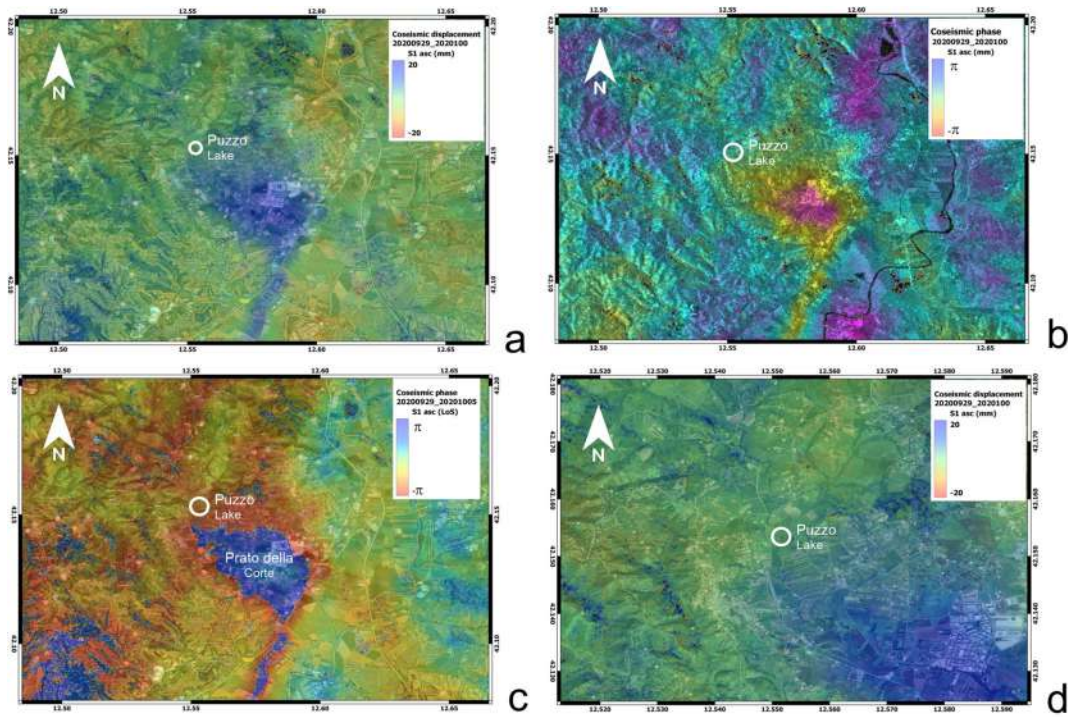
Forward modeling (Hinze, 2013) was carried out on the described Bouguer dataset using GMSYS software by Geosoft (<https://www.sequent.com>), incorporating 100 data points from the data grid of the Fig. 6b. The 2.75D modeling crosses the study area along profile PP', perpendicular to the field maximum elongation positioned near the Lago Puzzo, and was conducted to estimate the potential depth of the carbonate bedrock.

3.5. Resistivity Measurements

The electrical resistivity measurements were carried out along the accessible eastern and north-eastern sides of the Lago Puzzo, also in correspondence with the linear, circular, and pseudo-elliptical features previously described and observed in the aerial photographs (Fig. 7c–e and in Fig. 3c–e). The shorter ERT profiles 1 and 2 were conducted in correspondence to the circular forms lying in the gentle central slope of the plateau, a few tens of meters from the lake (Fig. 7b and c). The measurements were executed with 48 electrodes placed 1 m apart and with a total array length of 48 m in order to investigate the shallowest portion of the subsurface (c.a. 10–15 m below the ground). The longer ERT profiles ERT3 and ERT4 were positioned to intersect the linear fracture observed at the northeastern side of the plateau and to characterize the electrical properties of its southeastern side, respectively (Fig. 7d and e). Both these latter profiles used 48 electrodes with 5 m electrode spacing, covering a total length of 240 m and reaching an investigation depth of about 52 m below the ground.

The measurements were undertaken using the IRIS Syscal Pro Switch geo-resistivimeter. The elevation of the electrodes was measured with the

Assessing the Impact of the October 2020 Capena Earthquake



◀Figure 5

InSAR analysis—Sentinel-1 ascending orbit: co-seismic displacement (in mm, panel **a**) and co-seismic wrapped phase detected between September and October 2020 (panels **b–c**). Panel **c** highlights the “Prato della Corte” co-seismic uplift area at the center of the map. Multitemporal displacement analysis: close-up of the Lago Puzzo area, showing ground deformation from April 6, 2016 to September 23, 2023 (in mm, panel **d**). The white circle marks the location of Lago Puzzo. Total deformation in a zoomed-in area surrounding the lake (in cm, panel **e**). Deformation velocity profiles (in cm/year) relative to a reference Permanent Scatterer located south of the lake (its position is indicated by a small black square, panel **f**)

Stonex SA900 GPS receiver in RTK differential configuration, providing centimeter-level precision in orthometric height. The four profiles measured pseudo-resistivity using a Wenner-Schlumberger

array configuration. Effective resistivity sections were generated by inverting the apparent resistivity data with the RES2Dinv software, performing a “Robust” least-squares inversion (<https://www.geotomosoft.com>). This approach reduces the smoothness in parameter variation and of the derived properties during inversion. This technique is useful when investigating crustal sectors with sharp resistivity changes due to tectonic (faulting) or stratigraphic contacts. The inversion was performed using a mesh accommodating the topographic variations, which are generally modest for the ERT 1, ERT 2 and ERT 3 profiles, and more pronounced for the ERT 4 one. Figure 7 shows the pseudo-sections and the inversion results with real resistivity together with the topographic surface. In Fig. 8c–e the ERT tomographies are also shown with a different color

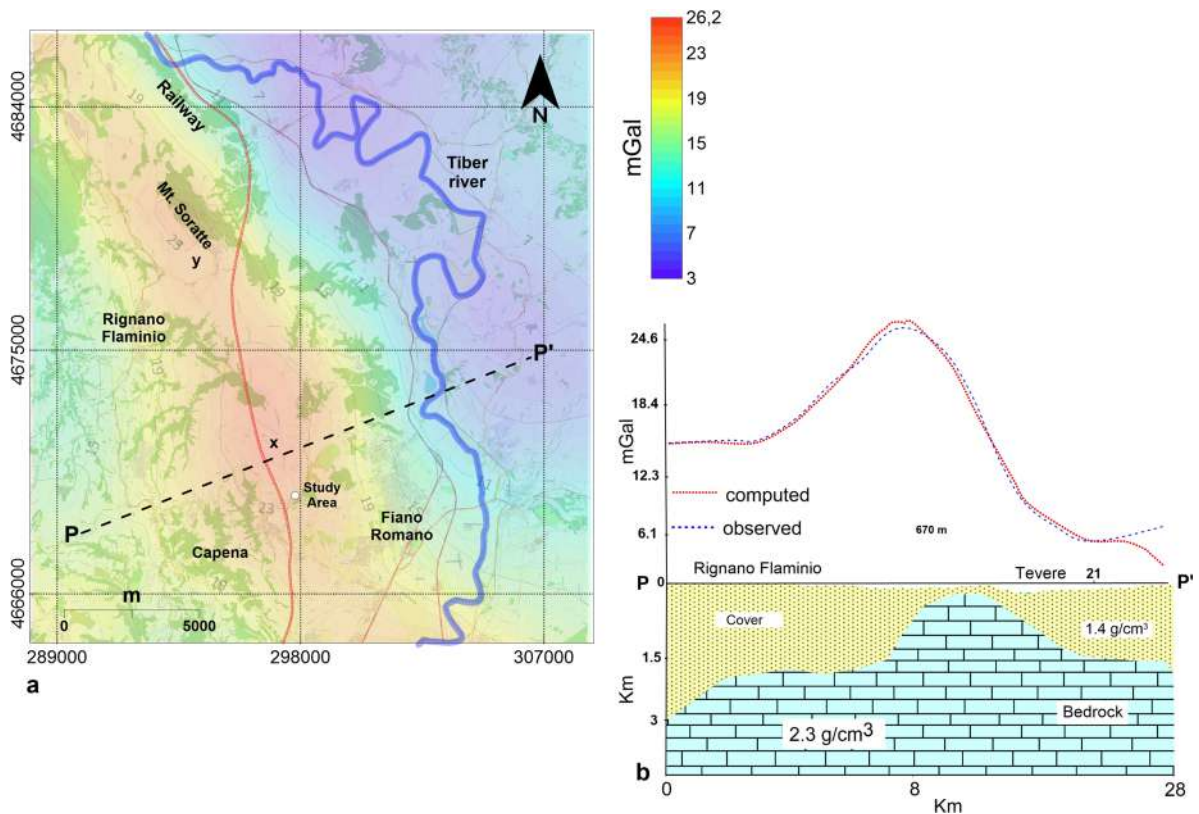


Figure 6

Regional Bouguer anomaly map (covering an area of 21 km east–west and 22 km north–south), overlaid on OpenStreetMap imagery (<https://tile.openstreetmap.org>). The ENE–WSW trending PP' profile (18 km long, panel **a**) is centered on the main Bouguer anomaly peak, located a few hundred meters from the Lago Puzzo plateau (panel **b**). The corresponding forward gravity model and geological reconstruction along the PP' profile are shown in panel **c**

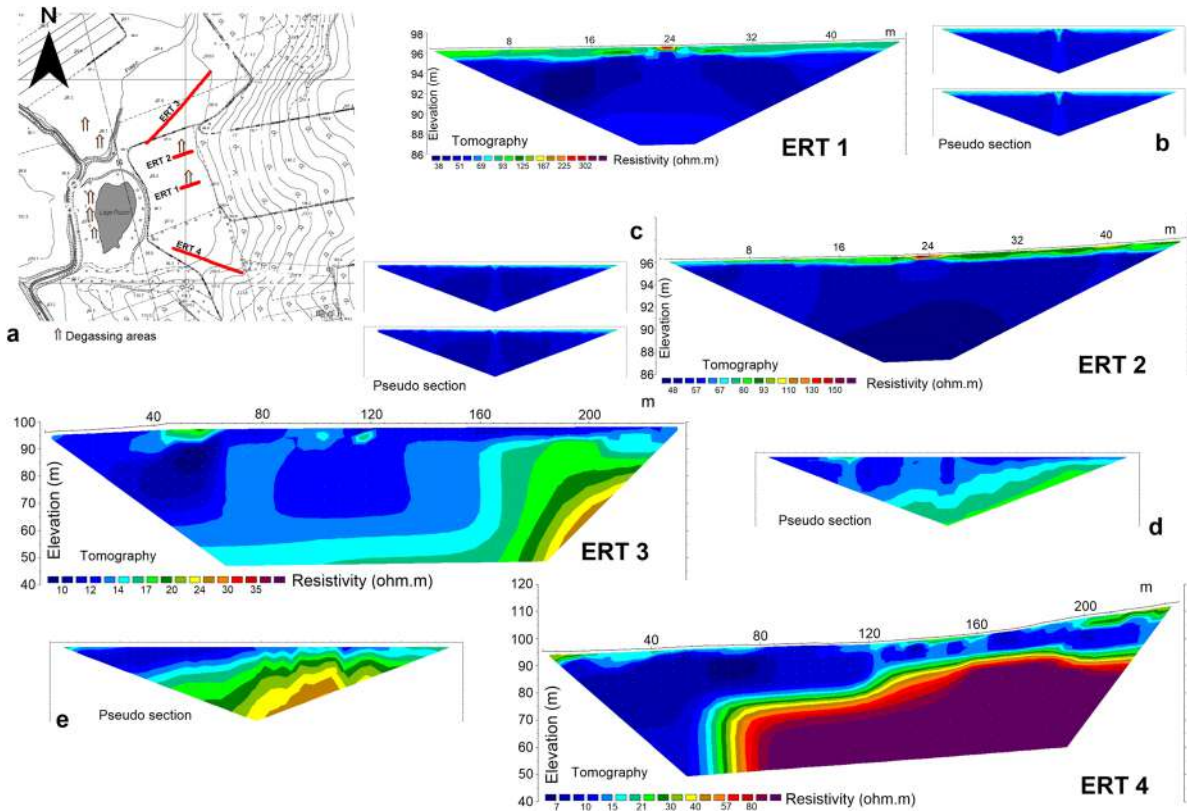


Figure 7

Electrical Resistivity Tomography (ERT) profile locations along the eastern side of the Lago Puzzo plateau, overlaid on the Topographic Map (Technical Regional Map—CTR, 1:10,000 scale, panel a). Inverted resistivity sections for ERT profiles 1, 2, 3, and 4, shown alongside their corresponding measured apparent resistivity data (smaller panels, b–e)

scale and vertical to the horizontal ratio which enhances the perception of the electro-stratigraphic structures. These figures show the profile interpretation, codified by different electro-strata patterns and letter numbering.

4. Result

4.1. Morphologic Analysis

The Lago Puzzo has a flattened ellipse shape with the 245 m long major axis striking N15E and the minor axis of about 115 m. Currently, the lake is partially filled with water (Figs. 1c and 3d). The lake is bordered by gentle, low-gradient hills (Fig. 3a) striking N-S, NNW-SSW, NNE-SSW, and E-W, with elevation ranging from 95 m (Lake Puzzo) to 220 m

asl with low Slope gradients (Fig. 3b). The hills flank a central plateau also elongated in the NS direction and with a lateral extent of about 1.4 km (Fig. 3a, b). This gently sloping plateau is crossed by the Fosso di S. Martino and its tributary (Fig. 1c) and hosts the Lago Puzzo inside a depressed sector bordered to the south by an E-W morphologic ridge (116 m asl.). The landscape is thus marked by alternating alignments, predominantly striking along the Apennine direction. This framework is even obvious in the Slope map (Fig. 3b) with a color scale ranging from red (steeper) to blue (lower). Although the topographic gradients are generally low, the DEM and its Slope Map provide a clear representation of the elongation directions of the hilly reliefs.

The analysis of the Google Earth aerial photo time series (Image © Maxar Technologies, covering observations from 2006 to 2022) revealed linear,

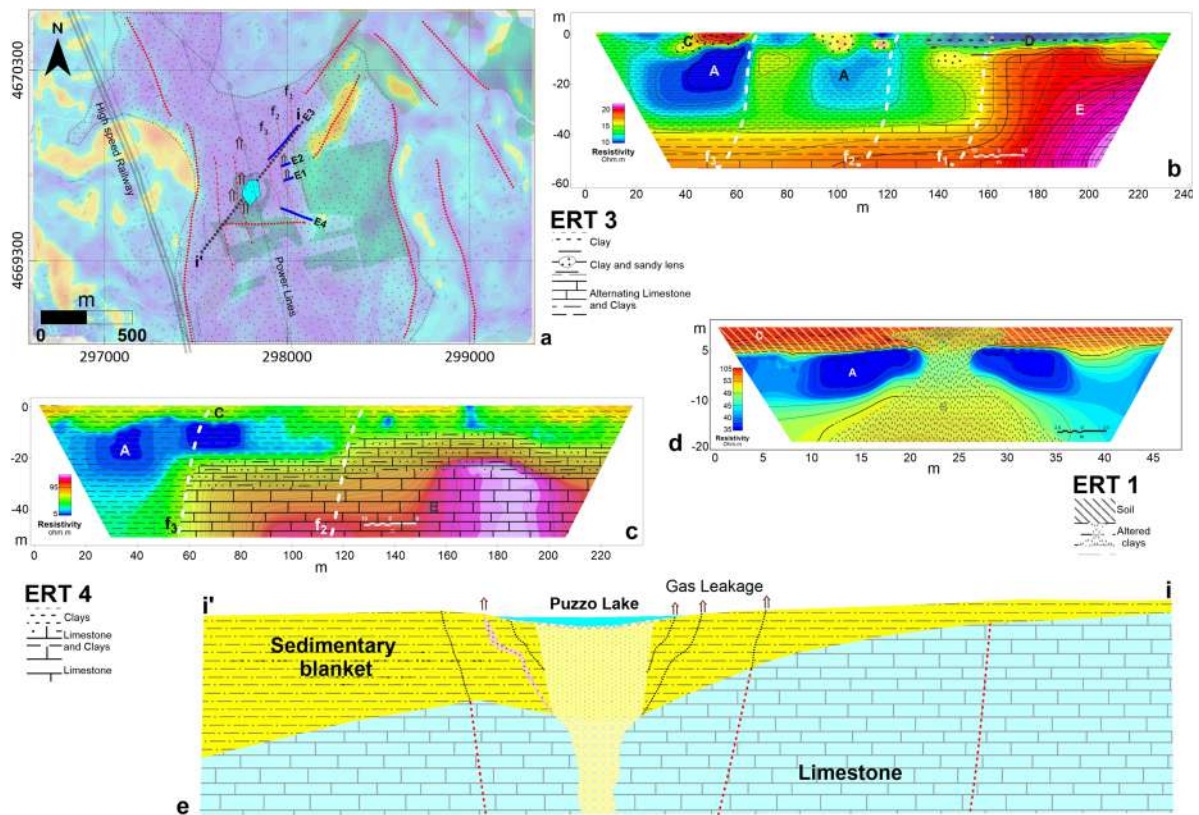


Figure 8

Fracture map of the Lago Puzzo plateau and surrounding area, derived from field observations, literature, aerial imagery, and geophysical data, overlaid on the slope map shown in Fig. 3b (panel a). Geological interpretations of ERT profiles 1, 3, and 4 (panels b–d). Reconstructed geological model of the Lago Puzzo sinkhole along the i-i' track of panel a (panel e)

circular, and pseudo-elliptical structures near the Lago Puzzo (Fig. 3c–e). These features, clearly observable in 2010 up to 2019 pictures (Fig. 3d), vary in their visibility depending on the season, lighting conditions, and vegetation growth at the time of the photo shoot. The significance of these features is further analyzed in the Discussion paragraph.

On the plateau's north-eastern side, a straight linear feature develops radially to the lake for nearly 400 meters and with the same strike of the tributary valley placed at the northernmost border of the plateau (Figs. 1c and 3c). Moreover, circular features occur close to the river bordering the lake. These latter are densely clustered especially on the lake's western side, often changing position. Unlike the other sides of Lago Puzzo, the northern one is characterized by the constant presence of cultivated agricultural land throughout the entire observational

period. On the northeastern side, however, the described features can also be observed at a greater distance from the lake close to the above described linear form (photo from 2019 in Fig. 3).

4.2. Seismological Analysis

Seismological analysis was conducted on the seismograms (velocity in m/s) recorded at the Monte Soratte (SRES), Montecelio (MTCE), and Santa Maria delle Mole (SAMA) stations of the Italian National Seismic Network (Fig. 4). Each station displays the three components of the seismic signal (EW, NS, Z). Fig. 4c and c show seismograms (velocity in m/s) from the MTCE station for two additional minor events near the Capena earthquake epicenter, recorded on 01/12/2020 (ML 1.5) and 12/04/2020 (ML 1.9), for comparative purposes.

Notably, the duration of the Capena earthquake signal extends beyond 20 seconds (Fig. 4b), whereas the other two events do not exceed 10 seconds. The extended duration of the Capena event is attributed to surface waves following the arrival of the S waves. Additionally, the anomalous duration of this event is noteworthy, as it cannot be attributed to local site effects; this behavior is consistent across all three recording stations (SRES, MTCE, and SAMA, Fig. 4a, b), which are situated in different geo-structural settings. Therefore, these characteristics likely reflect the intrinsic features of the seismic source itself.

Another characteristic feature of the Capena earthquake seismogram is the presence of low-frequency waves (Fig. 4e), contrasting with the high-frequency waves observed in the other two events. Typically, high-frequency components are characteristic of small tectonic earthquakes. Figure 4e provides a clearer representation of the frequency content of the three earthquakes we used for comparison, showing both seismograms and spectrograms of the motion components (MTCE station). The spectrograms emphasize the spectral differences of the Capena event whose spectral content is limited to approximately 5 Hz, with the most energetic portion of the signal associated with the S wave and subsequent surface waves. In the other two events, the maximum spectral energy reaches around 10 Hz, with the most energetic part occurring between the P and S wave arrivals.

Tectonic earthquakes are characterized by high-frequency signals linked to strong fault ruptures, whereas fluid-induced events, such as those from volcanic or geothermal activity, exhibit low-frequency signals (Calderoni et al., 2019). The attenuation of seismic waves by fluids reduces their frequency, making it a key factor in differentiating these phenomena. Spectrograms effectively emphasize these frequency variations.

4.3. InSAR Analysis

For the Sentinel-1 satellite analyses, the interferometric processing of SAR (InSAR) data for the co-seismic and pre-seismic phases does not indicate significant deformation phenomena across the

broader Capena regional area, specifically in the Fosso di San Martino watershed where historical sinkholes (e.g., Lago Nuovo, Fontana Ciocci) developed along NS-oriented tectonic lines. In the area of Lake Puzzo, a marked lack of PS is due to the presence of agricultural land. However, some subsiding pixels (negative velocity values) have been detected about 400-500 meters off the lake's shores, showing more evident subsidence in recent months compared to the previous period (Fig. 5f).

More generally and to a wide extent, a slight difference in the total number of uplifting PSs on the right side of the San Martino Valley surrounding the western flank of the plateau (experiencing slight uplift) and on the right side of the San Martino Valley surrounding the eastern flank of the plateau (undergoing a light subsidence) in terms of both total deformation and velocities (Fig. 5e). This observation warrants the need for further monitoring with time. Furthermore, about 5 km south of the Lake an uplift signal of approximately 1.5–2 cm is detected (Fig. 5c). However, it remains uncertain whether these signals are related to the earthquake, seismic-induced effects, or atmospheric artifacts. Additionally, in the “Prato della Corte area” (Fig. 5c) a co-seismic uplift is registered in the average ground velocity map. Instead, in the pre-seismic phase, strong subsidence occurred over the past four years with rates exceeding 3 cm/year. Given the local character of the observation (limited area extent) and its correspondence with a heavily industrialized zone, this phenomenon appears to be locally driven by anthropic activity, warranting further investigation. The post-seismic PS analysis over a period of nearly one year, does not reveal significant ground deformation, and movements have moderate intensity.

4.4. Gravimetry

The regional Bouguer anomaly map (Fig. 6a) is characterized by a prominent linear gravimetric height (x) extending in a north-south direction in the central portion of Fig. 6a but rotating to N40°W moving northward (y). These maxima exhibit sub-rounded to oblong-elliptical shapes with their major axes aligned in the NS and NNW-SSE directions, respectively. The first shape encircles the Capena

sinkhole-prone area, within which sinkholes have developed, (e.g., Lago Nuovo, Lago Vecchio, and Fontana Ciocci). The directional progression of sinkhole formation over time follows the x maximum elongation which in turn runs parallel to the structural trends (Fig. 2a). Moving northeast from the central Bouguer maximum, the field values decrease, and two NW-SE elongated minima are observed in correspondence with the Tiber graben.

Forward modeling in Fig. 6b highlights a density boundary between two units likely corresponding to the carbonate bedrock (2.3 g/cm^3 model density) and an overlying sedimentary/volcanic cover (1.4 g/cm^3 model density). This boundary has a depth ranging from about 100 m b.s.l. and a maximum of 3000 m b.s.l. on the western side of the profile. This interface is characterized by highs and lows in elevation, with the highest one positioned at the profile's center. Given the ENE-WSW orientation of the profile, the lower unit (the bedrock), is expected to continue beyond its extremities along the profile direction. The central section of the profile intersects approximately 800 meters from Lago Puzzo.

4.5. ERT Tomographies

Profiles 1 and 2 (Fig. 7b and c). The inversion of the pseudo-resistivity data shows a low root mean square error (0.44 and 0.25, respectively), and the results converge easily after 5–6 iterations. These ERT tomographies are characterized by a sub-horizontal electro-layers, interrupted by a plume-like structure positioned (also in the pseudosection) in the central part of the profile and in correspondence of the circular features identified at the surface.

In ERT Profile 1 (Figs. 7b and 8d), the plume is outlined at depth by the central B electro-layer, which exhibits slightly higher resistivity (49–50 ohm.m) and is laterally confined by the lower-resistivity A layers (36–45 ohm.m, Fig. 8d). At the surface, the tomography reveals higher resistivity values in layer C (60–430 ohm.m), with peak values concentrated in the central part of the profile. In the ERT 2 tomography (Fig. 7c), the previously described electrical scheme is less developed. At depth, slightly higher-resistivity electro-layers (55–62 ohm.m) form globular structures approximately 1 to 6 meters below

the surface. Conversely, the high-resistivity surficial electro-layer (57–185 ohm.m) follows a pattern similar to that of Profile 1, with the highest resistivity values also concentrated in the central part of the profile.

Profile 3. The inversion of pseudo-resistivity data also shows a low root mean square error (0.58), with the results converging after 5 iterations. The resulting ERT 3 tomography presents an articulated pattern characterized by two main sectors (Figs. 7d and 8b). The northeastern sector is characterized by the electro-layer E, with higher resistivity values (15–22 ohm.m) extending from 5 m below ground to the base of the tomography and spanning the entire profile length. The resistivity values gradually decrease toward the center and the southwestern sectors of the tomography where the layer unit A lies (8–12 ohm.m). Particularly, the tops of units A and E are at the same depth level. Above A and E, the surficial layer C, characterized by slightly higher resistivity (15–18 ohm.m), occurs in some patches. More in general, the resistivity range of the Profile 3 tomography is limited. However, the boundaries geometry between observed electro-layers are sharp with vertical dip.

Profile 4 (Figs. 7 and 8c). The inversion of pseudo-resistivity data of Profile 4 achieves a low root mean square error (0.49) and convergences after 6 iterations. The resulting tomography shows a clear electro-stratigraphic pattern, both in terms of electro-layer geometries and resistivity variation (Figs. 7e and 8e). The electrical schema consists of three main units. The electro-layer A (6–8 ohm.m), with very low resistivity, develops between 2–40 m below the ground in the north-western and central sectors of the tomography. In the remaining sectors, it becomes shallower and lies between 0–18 m. Electro-layer E, with higher resistivity (50–125 ohm.m), extends through most of the section between 10–50 m below the ground, forming a complex stepped roof. Finally, electro-layer C (15–35 ohm.m) lies in the surficial part of the profile. The contact between electro-layers A and E has a vertical dip, geometry which also appears to characterize an inner steep-like morphology of the unit E.

5. Discussion

The San Martino Valley is a subsided basin formed above a downthrown carbonate bedrock, overlain by a thick Plio-Pleistocene sedimentary sequence. It represents the surface expression of a high-angle \sim N–S trans-extensional fault, which connects the bedrock, sediments, and surface water, as supported by multi-scale geomorphological, geochemical, and geophysical evidences. Moreover, fluids of deep origin, rich in gas, rise along the fault plane, feeding a series of modest flow springs located along the Fosso S. Martino (Faccenna, 1994).

Seismic analysis of the October 20, 2020 event suggests the Capena earthquake—occurring at the onset of the rainy season—may not have been purely tectonic in origin (i.e., related solely to active fault movement). The notably longer duration of its seismogram, compared to those of two other earthquakes recorded in the same area (Fig. 4a), is attributed to the presence of surface waves following the S-wave arrival. These wave components may reflect subsurface processes triggered by the seismic event itself, potentially accounting for the rumbling sounds reported by local residents after the main shaking. Moreover, earthquake shaking is a critical and triggering factor in a sinkhole-prone areas, as it can accelerate the nucleation processes of new occurrences.

An experimental study (Lamb et al., 2021) shows that acoustic waves were generated by earthquakes during a hydraulic stimulation project in Finland, with frequencies ranging from the infrasonic (< 20 Hz) to above the lower threshold of human hearing (20–70 Hz). The audible sounds were described as dull noises or booms, similar to those reported by the residents of Capena, and were associated with shallow earthquakes (< 2 km depth). The study suggests that these audible noises are generated by local ground reverberation during the arrival of shallow seismic waves. A similar study was conducted in Texas by Schaible et al. (2023). These studies provide evidence that even low-magnitude earthquakes can generate sounds perceivable in the human audible range, especially when they are shallow and occur under geological conditions favorable to the propagation of acoustic waves. On the other hand, there is

wide literature correlating seismic events with acoustic phenomena (AE) observed in the ultrasonic band, and the reported Capena events may represent a portion of a broader frequency spectrum emitted during the earthquake (Zhu et al., 2024).

During this study, multiple inspections were conducted across the whole San Martino sinkhole-prone area in order to identify any surface rupture or ground collapse potentially triggered by seismic shaking. The extensive surveys did not reveal evidence of newly forming sinkholes. Moreover, we also reviewed all the possible noise sources without finding any natural and anthropogenic cause.

Upon completion of the first round of field inspections, we focused our attention on the Lago Puzzo. This site represents the most recent—and prominent—surface expression, located near the top of the carbonate basement, of the historical southward migration of sinkholes and, consequently, of the subsurface processes driving their formation. To support the analysis, we harnessed SAR interferometry across the broader regional area in order to detect possible co-seismic and pre-/post-seismic ground deformation. Although the limited density of PS near Lago Puzzo constrains the analysis, the available points along the San Martino Valley exhibit minimal variation throughout the observation period. However, there is a subtle difference between the PS deformation of the eastern (subsidence) and western (uplift) flanks of the valley surrounding the Puzzo lake (Fig. 5e). While this pattern lies at the edge of statistical significance, it highlights the importance of continued monitoring over time.

On the local scale, the geoelectrical investigation carried out in the Lago Puzzo plateau shows a clear evidence of vertical discontinuities. In ERT 3, these latter are not particularly prominent with respect to resistivity variations (about 30 ohms.m between the A–C–E electro-layers, Figs. 7d and 8c) but extend across the whole section depth (f1, f2, and f3). The low resistivity difference suggests a boundary between clayey sediments and terrigenous facies of the uppermost part of the basal sequence. Particularly, one of these discontinuities coincides with the previously discussed fracture observed in the aerial photo (Fig. 3c). This fracture, in turn, is parallel to the NE–SW lake tributary ditch located to the northeast

of the study area (Figs. 3a and 8a). In ERT 4, two step vertical discontinuities occurs in correspondence of a prominent topographic slope change (f1 and f2 in Figs. 7d–e and 8b, c) in the northwestern side of the profile. Here, two N-S and E-W striking hills intersect. In this profile, the resistivity variation is sharper (about 280 ohm.m between the A-E electro-layers, Figs. 7d and 8e) suggesting an electrical boundary between limestone and clayey sediments. It is worth noting that the electrical discontinuities observed in ERT4 likely represent the southward continuation of that identified in the ERT3 (f2 and f3 in Fig. 8a–c). According to our interpretive model, these discontinuities correspond to vertical fractures, interpreted as the uppermost expression of a buried fault system connecting the bedrock to the surface (Fig. 8b). Moreover, the observed ground features (Fig. 3d, e), ranging from circular to elliptical geometry, are the expression of occasional gas leakage along chimneys formed within the revealed fracture system. In fact, in correspondence with these features, within the first 10 meters of depth, the ERT1 and ERT2 tomographies (Figs. 7b, c and 8d) show the typical electrical plume-like structures (Fig. 8d) consistent with marks of similar processes documented in other geological contexts (Sciarra et al., 2021). The above observations support the existence of pervasive fracturing and degassing around the lake (Fig. 3c–e). In addition to that, on the western side of Pozzo Lake, the scorched patches tend to align along a N–S orientation, coinciding with the dominant strike of regional tectonic lineaments, suggesting that gas ascent follows structurally controlled fracture pathway (Fig. 8a).

On a wider scale, the gravimetric map of Fig. 6a shows a Bouguer anomaly maximum, belonging to the broader regional gravimetric lineament extending about 70 km along the Apennine axis and aligning to the north with the Mt. Soratte horst (Fig. 2a). In the study area, this anomaly trends NS and lies between the Sabatino and Tiber grabens. In the central portion of the forward model of Fig. 6b, in correspondence with the anomaly maximum, the carbonate bedrock upper surface rises to depths less than 100 m and deepens towards the southwestern and northeastern edges of the profile. On the southwestern side, the surface slope is steeper, whereas on the northeastern

side, it is gentler. However, both slopes gradually stabilize at depth, leveling out approximately 6 km from the central axis maximum. This slope asymmetry suggests a significant tectonic downthrow along the southwestern side. Our interpretative model characterizes the area as being strongly influenced by tectonic activity, with a carbonate basement rising steeply to the east, and slowly deepening eastward, after reaching shallow depths. The depicted characteristics support the earlier findings of Bortolani and Carugno (1979), which noted the carbonate bedrock shallowing on the left bank of the Fosso di S. Martino and its rapid deepening on the right bank, a few km south of Mt. Soratte.

At the surface, the Fosso di San Martino broadens near Lago Pozzo, forming a plain up to 1,400 meters wide. This widening is most likely related to the basement morphology, which likely features a small graben, bounded by minor elevated blocks (low hills) and controlled by N-S and E-W lateral fracturing (Fig. 8a). This configuration is also consistent with the development of a small pull-apart basin, as described within the strike-slip model proposed by Faccenna and Funicello (1993). The fractures surrounding the Lago Pozzo are likely influenced also by the stress field associated with its formation. However, they are probably directly connected to deeper faults of the Mesozoic basement, creating a direct and efficient link to the local and regional hydrogeological systems. This connection is evidenced by the widespread degassing phenomena (Fig. 8b).

The presence of a sinkhole-prone area along the Fosso di S. Martino, near the epicentral area—where similar features to the Lago Pozzo have developed in historical times (including large occurrences, as noted by Nisio and Del Prete, 2008)—alongside a regional tectonic element with an NNW-SSE orientation (Bortolani and Carugno, 1979) and shallow bedrock, suggest the existence of a highly karstified carbonate sequence close to the surface. Moreover, in this context, the above-mentioned abrupt/gentle depth change of the bedrock towards the west and east respectively (Bortolani and Carugno, 1979), may favor high hydraulic gradients during the rainy season between the top of the buried bedrock (in the uplifted sector of the right hand of the Tiber river bank) and

the Tiber base level. This condition may imply a potential high energy of the hydrogeological system.

6. Conclusions

The October 2020 Capena earthquake exhibited spectral characteristics suggesting the involvement of mechanisms beyond simple tectonic faulting. The detection of low-frequency waves in the spectral data supports the hypothesis of dynamic processes occurring within the carbonate basement. These may include hydraulic phenomena—such as water hammer effects in the hydrogeological system—as well as collapses or mass movements along slopes or cave walls within a buried karst setting. Although establishing a direct causal link between the seismic event and the prolonged audible noise signals reported by local witnesses during the Earthquake remains challenging, their near-simultaneous occurrence strengthens the hypothesis of a cause-and-effect relationship. Regional-scale SAR interferometry indicates overall ground stability, with only minor differential displacements observed across the valley. Gravimetric, electrical, and morphological data collectively point to a shallow carbonate bedrock, faulting patterns consistent with the regional tectonic framework, and vertical active fracturing associated with gas emissions. The area appears to correspond to a locally subsided structural depression—a small graben—within a basement that rises toward the east. Given the spatial and temporal distribution of large sinkholes in the region, the carbonate substratum is interpreted as highly karstified and prone to continued, long-term subsurface activity. These findings provide evidence that the Lago Puzzo sinkhole remains morphologically active and potentially susceptible to further reactivation through new fracturing. Taken together, these considerations highlight the importance of sustained multidisciplinary monitoring, particularly through the integration of remote sensing techniques. Ultimately, this analysis offers a descriptive baseline that may serve as a reference framework for future investigations.

Acknowledgements

We thank the municipal authority for accompanying us during inspections and surveys across the entire area to assess the sites conditions. We also thank the landowners for granting us access to their properties to conduct the measurements.

Author Contributions RDR: Project leader, planning and measurements execution, onsite inspections data modeling, interpretation, and article writing. GR: Project leader: onsite inspections, measurements execution, interpretation. CT: InSAR data analysis and interpretation. GC: October 4th 2020 earthquake sesimological analysis and interpretation. FM: regional and geological and geomorphological analysis and interpretation. AA, MC: funding body for the investigations, onsite inspections, logistic support, and interpretation. PV, MF: measurements execution.: CD: model discussions and interpretation. All authors reviewed the manuscript.

Funding

Open access funding provided by Istituto Nazionale di Geofisica e Vulcanologia within the CRUI-CARE Agreement. This study was funded by the “Città Metropolitana di Roma Capitale (CMRC)” and conducted as part of the two-year INGV-CMRC project focused on the geophysical characterization of areas at risk of sinkholes near roads and infrastructures under the jurisdiction of the CMRC.

Data Availability

APA: (ISPRA, n.d.). Carta Gravimetrica alla scala 1:1.250.000: <https://www.isprambiente.gov.it/it/attivita/suolo-e-territorio/cartografia/carte-geofisiche-a-piccola-scala/carta-gravimetrica-alla-scala-1-a-1250000>, NASA Jet Propulsion Laboratory (2000). Shuttle Radar Topography Mission (SRTM) Global 1 Arc-Second dataset. NASA EOSDIS Land Processes DAAC. Available at: <https://doi.org/10.5067/MEaSURES/SRTM/SRTMGL1.003>.

Declarations

Conflict of interest The Authors have no conflicts of interest to declare that are relevant to the content of this article.

Open Access This article is licensed under a Creative Commons Attribution 4.0 International License, which permits use, sharing, adaptation, distribution and reproduction in any medium or format, as long as you give appropriate credit to the original author(s) and the source, provide a link to the Creative Commons licence, and indicate if changes were made. The images or other third party material in this article are included in the article's Creative Commons licence, unless indicated otherwise in a credit line to the material. If material is not included in the article's Creative Commons licence and your intended use is not permitted by statutory regulation or exceeds the permitted use, you will need to obtain permission directly from the copyright holder. To view a copy of this licence, visit <http://creativecommons.org/licenses/by/4.0/>.

Publisher's Note Springer Nature remains neutral with regard to jurisdictional claims in published maps and institutional affiliations.

REFERENCES

- Argentieri, A., Carluccio, R., Cecchini, F., Chiappini, M., Ciotoli, G., De Ritis, R., & Venuti, A. (2015). Early stage sinkhole formation in the Acque Albule basin of central Italy from geophysical and geochemical observations. *Engineering Geology*, 191, 36–47. <https://doi.org/10.1016/j.enggeo.2015.03.010>
- Bense, V. F., Gleeson, T., Loveless, S. E., Bour, O., & Scibek, J. (2013). Fault zone hydrogeology. *Earth-Science Reviews*, 127, 171–192.
- Berardino, P., Fornaro, G., Lanari, R., & Sansosti, E. (2002). A new algorithm for surface deformation monitoring based on small baseline differential SAR interferograms. *IEEE Transactions on Geoscience and Remote Sensing*, 40(11), 2375–2383. <https://doi.org/10.1109/TGRS.2002.803792>
- Billi, A., De Filippis, L., Poncia, P. P., Sella, P., & Faccenna, C. (2016). Hidden sinkholes and karst cavities in the travertine plateau of a highly-populated geothermal seismic territory (Tivoli, central Italy). *Geomorphology*, 255, 63–80.
- Bortolani, L., & Carugno, P. (1979). Lineamenti geologico-strutturali dell'area a sud del Monte Soratte (Lazio centro-settentrionale). *Bollettino della Società Geologica Italiana*, 98, 353–373.
- Caramanna, G., Ciotoli, G., & Nisio, S. (2008). A review of natural sinkhole phenomena in Italian plain areas. *Natural Hazards*, 45(2), 145–172. <https://doi.org/10.1007/s11069-007-9165-7>
- Ciccacci, S., D'Alessandro, L. E. A. N. D. R. O., Fredi, P., & Lupia Palmieri, E. (1988). Contributo dell'analisi geomorfica quantitativa allo studio dei processi di denudazione nel bacino idrografico del Torrente Paglia (Toscana meridionale–Lazio settentrionale). *Geografia Fisica e Dinamica Quaternaria*, (1), 171–188.
- Calderoni, G., Di Giovambattista, R., Pezzo, G., Albano, M., Atzori, S., Tolomei, C., & Ventura, G. (2019). Seismic and geodetic evidences of a hydrothermal source in the Md 4.0, 2017, Ischia earthquake (Italy). *Journal of Geophysical Research: Solid Earth*, 124, 5014–5029. <https://doi.org/10.1029/2018JB016431>
- De Ritis, R., Nardi, A., Materni, V., Venuti, A., Stefanelli, P., Rotella, G., & Chiappini, M. (2020). Multidisciplinary study of subsidence and sinkhole occurrences in the Acque Albule Basin (Roma, Italy). *Earth and Space Science*, 7(7), e2019EA000870. <https://doi.org/10.1029/2019EA000870>
- Di Loreto, E., Faccenna, C., Funicello, R., & Mattei, M. (1995). La valle del Tevere (Capena). In: *Memorie Descrittive della Carta Geologica d'Italia*, Vol. 85, pp. 33–132. Istituto Superiore per la Protezione e la Ricerca Ambientale (ISPRA).
- Faccenna, C., & Funicello, R. (1993). Tettonica pleistocenica tra il monte Soratte e i monti Cornicolani (Lazio). *Alpine and Mediterranean Quaternary*, 6(1), 103–118.
- Faccenna, C. (1994). Structural and hydrogeological features of Pleistocene shear zones in the area of Rome (Central Italy). *Annals of Geophysics XXXVII*, 1, 121–133.
- Ferretti, A., Prati, C., & Rocca, F. (2002). Permanent scatterers in SAR interferometry. *IEEE Transactions on geoscience and remote sensing*, 39(1), 8–20.
- Hinze, W. J., Von Frese, R. R., Von Frese, R., & Saad, A. H. (2013). Gravity and magnetic exploration: Principles, practices, and applications. *Cambridge University Press*. <https://doi.org/10.1017/CBO9780511843129>
- Hooper, A., Zebker, H., Segall, P., & Kampes, B. (2004). A new method for measuring deformation on volcanoes and other natural terrains using InSAR persistent scatterers. *Geophysical Research Letters*. <https://doi.org/10.1029/2004GL021737>
- Kaufmann, G. (2014). Geophysical mapping of solution and collapse sinkholes. *Journal of Applied Geophysics*, 111, 271–288. <https://doi.org/10.1016/j.jappgeo.2014.10.011>
- Lamb, O. D., Lees, J. M., Malin, P. E., & Saarno, T. (2021). Audible acoustics from low-magnitude fluid-induced earthquakes in Finland. *Scientific Reports*, 11(1), 19206.
- Marra, F., Florindo, F., Jicha, B. R., Nomade, S., Palladino, D. M., Pereira, A., Sottili, G., & Tolomei, C. (2019). Volcano-tectonic deformation in the Monti Sabatini Volcanic District at the gates of Rome (central Italy): evidence from new geochronologic constraints on the Tiber River MIS 5 terraces. *Scientific Reports*, 9, 11496. <https://doi.org/10.1038/s41598-019-47585-8>
- Micallef, A., Smith, M. J., Paron, P., & Griffiths, J. S. (2011). Geomorphological Mapping: Methods and Applications. *Developments in Earth Sciences*.
- NASA Jet Propulsion Laboratory. (2000). Shuttle radar topography mission (SRTM) global 1 arc-second dataset. NASA EOSDIS Land Processes DAAC. <https://doi.org/10.5067/MEASURES/SRTM/SRTMGL1.003>
- Nisio, S., Gracioti, R., & Vita, I. (2004). I fenomeni di sinkhole in Italia: terminologia, meccanismi genetici e problematiche aperte. *Proceeding: State of the art on the study of sinkhole phenomena and role of the national and local government in the territory administration*. Rome, 20–21 May 2004, pp 557–572.
- Nisio, S., Caramanna, G., & Ciotoli, G. (2007). Sinkholes in Italy: first results on the inventory and analysis of some case studies. *Geological Society, London, Special Publications*, 279(1), 23–45.
- Nisio, S. (2008). I Sinkholes nel Lazio. *Memorie della Società Astronomica Italiana*, 85, 33–148.
- Nisio, S., Del Prete, S., Guarino, P. M., Iovine, G., Parise, M., & Santo, A. (2008). I fenomeni naturali di sinkhole nelle aree di pianura italiane. *Memorie Descrittive della Carta Geologica d'Italia*, ISPRA, 85, pp. 482, Roma.

- Nof, R. N., Abelson, M., Raz, E., Magen, Y., Atzori, S., Salvi, S., & Baer, G. (2019). SAR interferometry for sinkhole early warning and susceptibility assessment along the Dead Sea, Israel. *Remote Sensor*, 11, 89. <https://doi.org/10.3390/rs11010089>
- Peccerillo, A. (2017). Cenozoic volcanism in the Tyrrhenian Sea region (p. 399). New York, NY, USA: Springer. <https://doi.org/10.1007/978-3-319-42491-0>.
- Rodriguez, E., Morris, C. S., Belz, J. E., Chapin, E. C., Martin, J. M., Daffer, W., & Hensley, S. (2005). An assessment of the SRTM topographic products, *Technical Report JPL D-31639*. Pasadena, California: Jet Propulsion Laboratory.
- Santo, A., Ascione, A., Del Prete, S., Di Crescenzo, G., & Santangelo, N. (2011). Collapse sinkholes in the carbonate massifs of Central and Southern Apennines. *Acta Carsologica*. <https://doi.org/10.3986/ac.v40i1.31>
- Schaible, L. P., Dannemann Dugick, F. K., & Bowman, D. C. (2023). Infrasound detections of low-magnitude earthquakes: preliminary results of the west texas acoustic experiment (No. SAND-2023-14433). Sandia National Lab. (SNL-NM), Albuquerque, NM (United States).
- Sciarra, A., Cantucci, B., Sapia, V., De Ritis, R., Ricci, T., Civico, R., & Coltorti, M. (2021). Geochemical and geoelectrical characterization of the Terre Calde di Medolla (Emilia-Romagna, northern Italy) and relations with 2012 seismic sequence. *Journal of Geochemical Exploration*, 221, 106678. <https://doi.org/10.1016/j.scitotenv.2024.171483>
- Sella, P., Billi, A., Mazzini, I., De Filippis, L., Pizzino, L., Sciarra, A., & Quattrocchi, F. (2014). A newly-emerged (August 2013) artificially-triggered fumarole near the Fiumicino airport, Rome, Italy. *Journal of Volcanology and Geothermal Research*, 280, 53–66. <https://doi.org/10.1016/j.jvolgeores.2014.05.008>
- Waltham, T., Bell, F. G., & Culshaw, M. G. (2005). *Sinkholes and subsidence: karst and cavernous rocks in engineering and construction*. Springer Science & Business Media.
- Zhu, Z., Jiang, Z., Accornero, F., & Carpinteri, A. (2024). Correlation between seismic activity and acoustic emission on the basis of in situ monitoring. *Natural Hazards and Earth System Sciences*, 24(11), 4133–4143.

(Received February 17, 2025, revised May 12, 2025, accepted August 11, 2025)